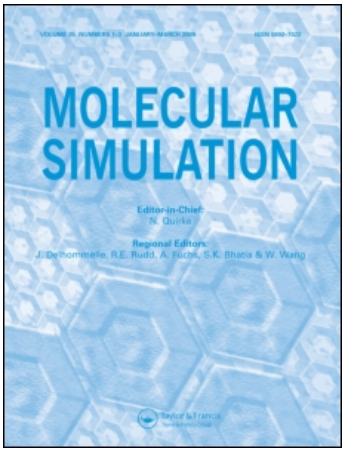


**Molecular Simulation**
Publication details, including instructions for authors and subscription information:
http://www.informaworld.com/smpp/title~content=t713644482

# Computer Simulation Study of the Chemical Potential of Argon Adsorbed on Graphite

Ailan Cheng[ab]; W. A. Steele[ac]
[a] The Pennsylvania State University, University Park, PA, USA [b] Department of Physics, [c] Department of Chemistry,

**To cite this Article** Cheng, Ailan and Steele, W. A.(1990) 'Computer Simulation Study of the Chemical Potential of Argon Adsorbed on Graphite', Molecular Simulation, 4: 6, 349 — 359
**To link to this Article: DOI:** 10.1080/08927029008022399
**URL:** http://dx.doi.org/10.1080/08927029008022399

*Molecular Simulation*, 1990, Vol. 4, pp. 349–359
Reprints available directly from the publisher
Photocopying permitted by license only



# COMPUTER SIMULATION STUDY OF THE CHEMICAL POTENTIAL OF ARGON ADSORBED ON GRAPHITE

AILAN CHENG* and W. A. STEELE**

*The Pennsylvania State University, University Park, PA 16802, USA*

(*Received September 1989, accepted November 1989*)

A multilayer film of argon adsorbed on the basal plane of graphite at 103 K was simulated using isokinetic molecular dynamics. The local chemical potentials in the film were evaluated using three algorithms suggested in the literature: test particle insertion, real particle calculation and the ratio method, which relies on calculations of the local energy distribution functions for test and real particles. Although none of these was suitable for calculations involving the partially solidified first adsorbed layer, the test particle and the ratio method produced useful results for regions in the film corresponding to second and higher layers. The ratio method is shown to be the most realistic, giving constant local chemical potentials of reasonably high precision for all points other than in the first layer.

KEY WORDS: Chemical potential, argon, graphite, adsorption.



## 1. INTRODUCTION

Various macroscopic observables are generated in computer simulation studies of dense phases. Among the thermodynamic properties evaluated in this way, chemical potential is one of the most difficult. In connection with simulations of physisorbed films, this is unfortunate, since there are several reasons why chemical potential is of particular interest in these systems. First, a standard experiment is to measure the adsorption isotherm, which is pressure (or fugacity) of the gas in equilibrium with a film of given amount adsorbed $n_a$. Such data yields values for the chemical potential $\mu^{ads}$ of the film as a function of coverage $\Gamma = n_a/\mathscr{A}$, where $\mathscr{A}$ is surface area. In fact, one can write

$$\mu^{ads} = \mu^{gas} = RT(\ln (P/kT) + \ln \Lambda^3) \tag{1.1}$$

where $P$ is the pressure of the (ideal) gas and $\Lambda = h/\sqrt{2\pi mkT}$ for a monoatomic adsorbate. Furthermore,

$$\mu^{ads} = RT\left[\left(\frac{\partial \ln Z(n_a)}{\partial N}\right)_{T,V} + \ln \Lambda^3\right) \tag{1.2}$$

where $Z(n_a)$ is the configurational integral for $n_a$ adsorbed atoms. The problem is to evaluate $Z$ and its derivative in a computer simulation with sufficient precision to yield meaningful value for $\mu^{ads}$ or $P$, the isotherm pressure. In addition to thermodynamic integration [1] a number of indirect methods for evaluating chemical potential have

*Department of Physics.
**Department of Chemistry.

been suggested over the past few years [2–6] and tested by simulations, primarily of Lennard-Jones liquids.

A second point of interest appears in multilayer adsorption viewed as inhomogeneous fluids produced by the strong external potential near the adsorbent surface.[7] This arises because the local chemical potential should be constant in such systems no matter where one chooses a small volume element for the calculation. For example, in such a film one could hope to determine whether the atomic configurations generated by simulation were those for a fully equilibrated layer by evaluating local chemical potentials for various regions and determining whether or not these potentials were the same for all layers. This is an even more difficult task than the evaluation of $\mu$ for the film as a whole, for the obvious reason that the numbers of atoms in small volume elements is much smaller than the total, leading to poorer statistics in a calculation that is plagued by poor statistics even when considering the fluid as a whole.

In this paper, we present a comparative study of some of the algorithms that have been suggested for simulating chemical potential. We attempt to evaluate local chemical potentials for a nominally three-layer film of argon on graphite. At the simulation conditions, the first layer is partially solid and the outer layers are dense liquids. We found that $\mu$ could not be successfully simulated for the first solid layer, in agreement with the findings of others, [8] but that reasonably reliable values could be obtained for the atoms in volume elements located at distances from the surface corresponding to layers more distant than the first. The results obtained will illustrate the strengths and weaknesses of the three algorithms utilized.



## 2. SIMULATION DETAILS

The Ar–Ar and Ar-graphite interaction laws used in these simulations are identical to those employed previously [9] and include representations of the periodically varying part of the Ar-solid potential as well as the substrate mediated alteration in the Ar–Ar potential for pairs of atoms in the layer closest to the solid. An isokinetic molecular dynamics algorithm was employed with the temperature set equal to 103 K.[10] The total number of atoms simulated was 600 in a box chosen to give $\sim$ 200 atoms per layer. Views of the center-of-mass trajectories that are shown in Figure 1 indicate that the first layer is partially melted under these conditions but the second and higher layers are fluid. Various contributions to the average potential energy per particle in each layer of the film are listed in Table I. These data were obtained by equilibrating the system for 20,000 timesteps (amounting to a time of 67 ps) and subsequently gathering data for 10,000 timesteps more. Data saved included configurational information (positions and velocities) for each of the atoms at intervals of 10 timesteps. For better precision in the chemical potential, the simulation was then run for another 10,000 timesteps. Another quantity often evaluated in adsorption simulations is the adsorbate density $\rho(z)$ in atoms per unit length, calculated as a function of gas-solid separation distance $z$ and summed over the entire surface. This quantity is crucial to the success of two of the chemical potential algorithms, and thus was evaluated with some care. Atoms were separated into bins of width $\Delta z^* = 0.1$, with $z^* = z/2.46$ Å, and averages were taken over the entire duration of the (equilibrated) simulation. Figure 2 shows the time-dependent number of atoms in each layer. Aside from thermodynamically required fluctuations, no drifts in these quantities are observed,

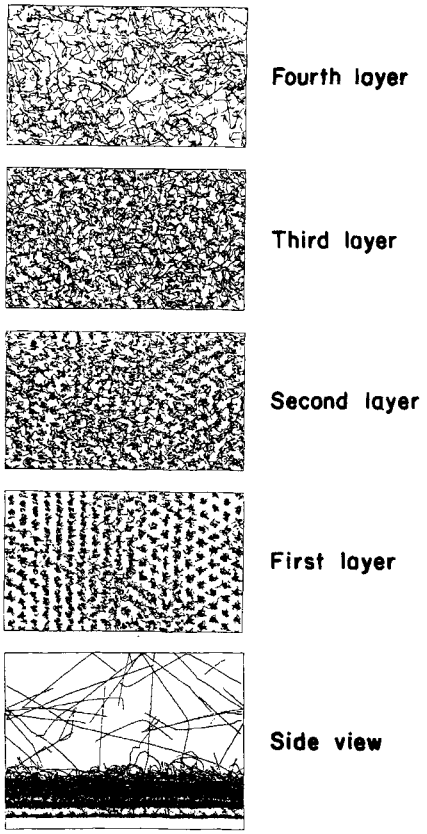


**Figure 1** Time-dependent trajectories of the atoms in the system simulated are shown in a side view (bottom panel) and in top views of the atoms in the first, second, third, and higher layers (sequentially upwards). A few desorbed atoms are seen in the side view – these are not included in the "higher layers".



giving one some confidence that the system is well equilibrated. The $z$-dependence of the time-averaged adsorbate density shown in Figure 3 indicates that the layer structure of this film is well maintained for the first three layers even though the temperature is well above the bulk melting point of 83.8 K.

**Table 1** Average simulation quantities. Energies are given in reduced units equal to energy/$\varepsilon_{Ar-C}$, where $\varepsilon_{Ar-C}/k = 57.9\,K$

| *Layer Number* | *Number of Atoms* | $\langle u^*_{gs} \rangle$ | $\langle u^*_{Ar-Ar} \rangle$ |
|---|---|---|---|
| 1 | 196 | −17.94 | −4.01 |
| 2 | 168 | −2.50 | −4.36 |
| 3 | 137 | −0.63 | −3.42 |
| 4 and higher | 98 | −0.20 | −1.46 |

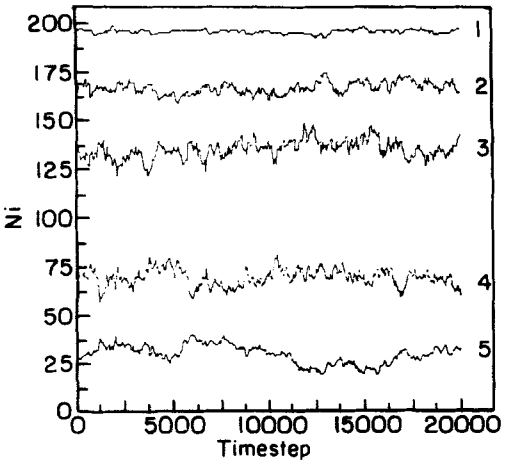


**Figure 2** The time dependence of $N_i$, the number of atoms in layer $i$ is shown here as a function of the number of timesteps. (1000 timesteps = 3.36 ps).



## 3. CHEMICAL POTENTIALS

The three algorithms studied here will be described as test particle, real particle and ratio. The first, which is perhaps the best known, [2,11,12] can be obtained for the local chemical potential in a small volume $\delta V(\mathbf{R})$ located at point $\mathbf{R}$ by writing

$$e^{-\mu/kT} = \frac{Z_N}{Z_{N-1}\,\Lambda^3 N} \tag{3.1}$$

where $Z_N$ is the configurational integral for the $N$ particles in the volume element at $\mathbf{R}$ and is thus

$$Z_N = \int\!\!\int\!\!\int_{\delta V(\mathbf{R})} \exp\,[-U_N/kT]\,d\mathbf{r}^N \tag{3.2}$$

with $U_N$ the total potential energy of the atoms with configuration $\mathbf{r}_1 \ldots . \mathbf{r}_N = \mathbf{r}^N$ in $\delta V$ and $d\mathbf{r}^N$ denotes integration over the positions of the $N$ atoms. Following the usual derivation of the test particle algorithm, one writes $U_N$ as

$$U_N = U_{N-1} + u_i(\mathbf{r}_N) \tag{3.3}$$

where $u_i(\mathbf{r}_N)$ is the energy of the $N$'th particle. Equation (3.1) can now be written as

$$e^{-\mu/kT} = \frac{\delta V}{Z_{N-1}\,\Lambda^3 N} \int\!\!\int\!\!\int_{\delta V(\mathbf{R})} e^{-(u_i(\mathbf{r}_N) + U_{N-1})/kT} d\mathbf{r}^{N-1} \tag{3.4}$$

However, the usual statistical mechanical expression for $\rho(\mathbf{R})$, [13] the singlet particle density at $\mathbf{R}$, can be substituted into equation (3.4) to show that

$$e^{-\mu/kT} = \frac{\langle BFT\rangle_{N-1,\mathbf{R}}}{\Lambda^3\,\rho(\mathbf{R})} \tag{3.5}$$

with

$$\langle BFT\rangle_{N-1,\mathbf{R}} = \frac{\int'''''_{\delta V(\mathbf{R})} e^{-(u_t + U_{N-1})/kT} d\mathbf{r}^{N-1}}{\int'''''_{\delta V(\mathbf{R})} e^{-U_{N-1}/kT} d\mathbf{r}^{N-1}} \tag{3.6}$$

Thus, $\langle BFT\rangle_{N-1,\mathbf{R}}$ denotes the Boltzmann factor for an added test particle, averaged over the configurations of $N-1$ particles in volume $\delta V(\mathbf{R})$. (In the present case, the volume element is a slab extending over the entire area of the simulation cell and a small interval of $z = \Delta z^*$.) We wish to calculate an accurate value of $\mu$ and in addition, to show that $\mu$ is a constant for all $z$ within the adsorbed film.

In the real particle method, one recognizes that

$$\left\langle e^{u_r(\mathbf{r})/kT}\right\rangle_{N-1,\mathbf{R}} = \frac{\int'''_{\delta V(\mathbf{R})} e^{-U_{N-1}/kT} d\mathbf{r}^{N-1}}{\int'''_{\delta V(\mathbf{R})} e^{-U_N/kT} d\mathbf{r}^{N-1}} \tag{3.7}$$

where $u_r(\mathbf{r})$ is now the $N$'th real particle in $\delta V$ so that

$$U_N = U_{N-1} + u_r \tag{3.8}$$

One uses the inverse of equation (3.1) to show that

$$e^{\mu/kT} = \rho(\mathbf{r}) \left\langle e^{u_r/kT}\right\rangle_{N-1,\mathbf{R}} \Lambda^3 \tag{3.9}$$

Other workers have demonstrated that this method of calculating chemical potential is not very accurate for bulk fluids; we will confirm that this is also true for the local $\mu$ in the present strongly inhomogeneous system.

The ratio algorithm [4] is based on simulations of the distribution of the potential energy of the particles in the volume element. For the $N$ particles in $\delta V(\mathbf{R})$, this distribution function is formally defined by

$$g(u, \mathbf{R}) = \frac{\int'''_{\delta V(\mathbf{R})} \delta(u - u_r)\, e^{-U_N/kT} d\mathbf{r}^{N-1}}{\int'''_{\delta V(\mathbf{R})} e^{-U_N/kT} d\mathbf{r}^{N-1}} \tag{3.10}$$

A second energy distribution is that for the test particle in a sample of $N-1$ atoms; this is defined by

$$f(u, \mathbf{R}) = \frac{\int'''''_{\delta V(\mathbf{R})} \delta(u - u_t)\, e^{-U_{N-1}/kT} d\mathbf{r}^{N-1}}{\int'''_{\delta V(\mathbf{R})} e^{-U_{N-1}/kT} d\mathbf{r}^{N-1}} \tag{3.11}$$

One uses equation (3.8) to show that

$$g(u, \mathbf{R}) = \frac{e^{-u/kT} \int'''''_{\delta V(\mathbf{R})} \delta(u - u_r)\, e^{-U_{N-1}/kT} d\mathbf{r}^{N-1}}{\int'''_{\delta V(\mathbf{R})} e^{-U_N/kT} d\mathbf{r}^{N-1}} \tag{3.12}$$

$$= \frac{e^{-u/kT} f(u, \mathbf{R})\, e^{\mu/kT} \Lambda^3}{\rho(\mathbf{R})} \tag{3.13}$$

Thus,

$$\ln\left(\frac{f(u, \mathbf{R})}{g(u, \mathbf{R})}\right), = \frac{u}{kT} - \frac{\mu}{kT} + \ln \frac{\rho(\mathbf{R})}{\Lambda^3} \tag{3.14}$$

As pointed out by Powles, *et al.* [4] a plot of $\ln f/g)$ versus $u$ should be linear with slope $1/kT$ and intercept $-\mu/kT + \ln \rho(\mathbf{R})/\Lambda^3$. From the simulated configurations, we have generated both $f$ and $g$ for the atoms in volume elements $\delta V(z)$. Thus, this algorithm can be evaluated as well as the test and real particle approaches.

## 4. RESULTS

First, we note that the need for evaluating chemical potential within a finite volume $\Delta z\mathscr{A}$ means that averages over the volume must be taken. In particular, averages of the density $\overline{\rho(z)}$ and the inverse density $\overline{\rho^{-1}(z)}$ were evaluated for various $z$ within the film. In the ratio method, $f$ and $g$ are averages over the volume $\delta V$; thus

$$\bar{f}(u, \mathbf{R}) = \frac{1}{\delta V(\mathbf{R})} \int_{\delta V(\mathbf{R})} f(u, \mathbf{R}')\, d\mathbf{R}' \tag{4.1}$$

and

$$\bar{g}(u, \mathbf{R}) = \frac{1}{\delta V(\mathbf{R})} \int_{\delta V(\mathbf{R})} \rho(\mathbf{R}')\, g(u, \mathbf{R}')\, d\mathbf{R}' \tag{4.2}$$

A second point is that none of the algorithms is capable of yielding useful results for $z$ corresponding to atoms in the first partially solid layer. This seems to be generally true for samples of high density and finite size, probably because the use of periodic boundary conditions eliminates important long wave-length density fluctuations needed for successful test and real particle evaluations. In any case, our analyses were limited to $z^*$ values ranging from 2.3 to 6.6 ($z^* = z/2.46$ Å). Widths of the volumes $\delta V$ were taken to be $\delta z^* = 0.05$ for the test and real particle algorithms, but $\delta z^* = 0.15$ was taken for the more detailed ratio calculation. The number of test particles inserted at random in each $\delta V$ was 490 for each configuration analyzed. The number of configurations taken were 1000 from a total of 10,000 timesteps.

Plots of $\langle BFT\rangle_{N-1,z}$ evaluated in this way are plotted together with $\overline{\rho(z)}$ in Figure 3, where it can be seen that the functions are proportional, but that the small values obtained for $z$ between layers means that the log of the ratio of the two functions will have considerable uncertainty there. In fact, $\langle BFT\rangle_{N-1,z}$ will also exhibit considerably larger uncertainty than for $\overline{\rho(z)}$ for the simple reason that each atom in $\delta V$ contributes to $\rho(z)$ but there is only one value for the Boltzmann factor of all atoms in the volume.

Values of chemical potential obtained for various $z$ from this test particle algorithm are plotted in Figure 4. The reason for the rather large scatter in the chemical potentials calculated this way can be seen by evaluating $f(u,z)$, the probability of finding a test particle with a given energy in the volume $\delta V(z)$. Note that chemical potential can also be viewed as the result of evaluating

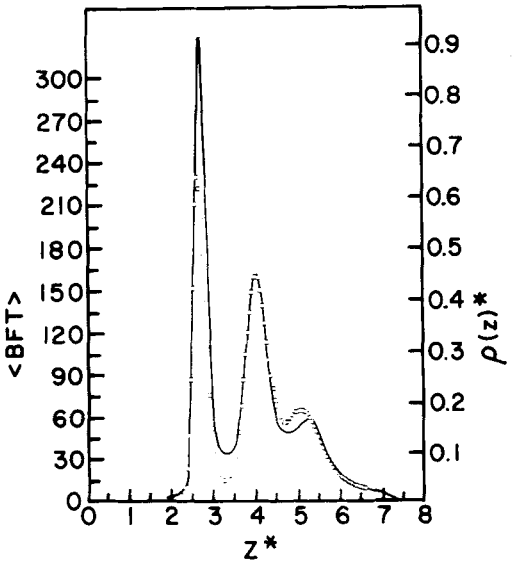


**Figure 3** The line shows surface density $\rho^*(z)$. The squares are values of the average Boltzmann factor test particle randomly inserted at a particular value of $z$. Reduced density $\rho^* = \rho\,(2.46\,\text{Å})^3$. If the chemical potentials evaluated by this algorithm was constant, the two curves would coincide at all $z$.

$$\langle BFT\rangle_{N-1,z} = \int_{-\infty}^{\infty} f(u,z)\, e^{-u/kT} du \tag{4.3}$$

In Figure 5, we show $f(u,z)$ and the integrand $f(u,z)\exp(-u/kT)$ for three values of $z$. When $z$ is small, one sees that the scatter in $f(u,z)$ is sufficiently large at relevant values of $u$ to give an average Boltzmann factor that will be quite uncertain. Furthermore, this difficulty becomes less significant as $z$ increases.

Chemical potential, the statistical uncertainty in $\mu$ and $g(u)$ were also evaluated for real particles in the volumes $\delta V(z)$. Much the same picture emerges: a local chemical

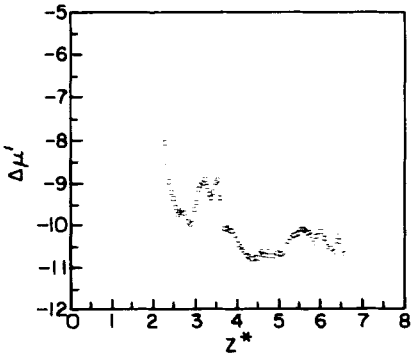


**Figure 4** Chemical potentials evaluated by the test particle method are shown for various values of $z^* = z/2.46\,\text{Å}$.

potential that apparently depends upon $z$. However

$$\frac{1}{\langle BFT \rangle_z} = \int g(u, z)\, e^{u/kT} du \tag{4.4}$$

for the real particle algorithm Plots of $g(u, z)$ and $g(u, z)\exp(u/kT)$ are shown in Figure 7 for three values of $z$. One can see that the integrand of equation (4.4) shows large scatter as one goes to positive values of $u$. Consequently, the $\langle BFT \rangle_z$ for small $z$ is expected to show the very large uncertainties shown in Figure 6.

For both the test and the real particle algorithms, the calculated chemical potentials are not of satisfactory constancy and precision. In both cases, the problem is caused by the fact that unlikely configurations corresponding to improbable $u$ values give large contributions to the chemical potential due to the exponential weighting factors at large negative $u$ for test particle calculation and at large positive $u$ for the real

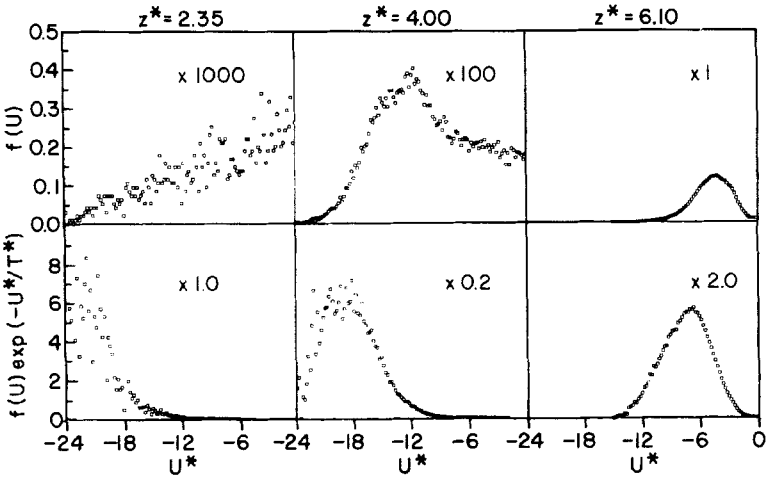


**Figure 5** This set of plots shows the energy distribution $f(u)$ and $f(u)\exp(-u/kT)$ for test particles inserted at three different values of $z^*$ shown at the tops of the panels. The numbers in each panel indicate multiplicative factors in the vertical scale of the plots relative to that shown along the left hand edge.

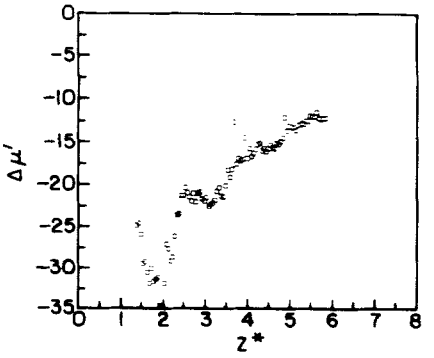


**Figure 6** The chemical potential calculated from the real particle algorithm are plotted for various values of $z^*$.

particle case. There seems to be no way to satisfactorily reduce the resulting uncertainty other than simulations that are orders of magnitude longer than those reported here.

However, the ratio algorithm holds some promise for avoiding this problem. What one requires is that $\ln[f(u,z)/g(u,z)] - u/kT$ be accurately constant over a limited range of $u$. Scatter in such a plot at the extremes is an obvious consequence of having either $f$ or $g$ become very small and thus can be excluded from the calculation. Such plots are shown in Figure 8 for the values of $z$ used in the test and real particle simulations. It is evident that regimes of $u$ exist where $\ln[f(u,z)/g(u,s)] - u/kT$ are close to a constant value. Furthermore, chemical potentials calculated in this way are reasonably independent of $z$ and do not show inordinate scatter, as is illustrated in Figure 9.

## 5. CONCLUSIONS

In common with other attempts to evaluate local chemical potentials in dense fluids by direct stimulation, we find that: 1) none are quantitatively useful for a solidified

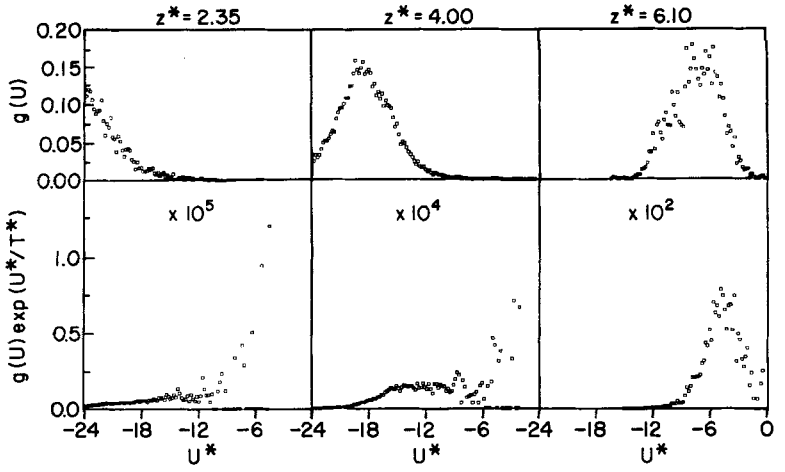


**Figure 7** These plots show the energy distribution $g(u)$ and $g(u)\exp(u/kT)$ for the real particle algorithm. The numbers are multiplicative factors for the vertical scales of the plots.

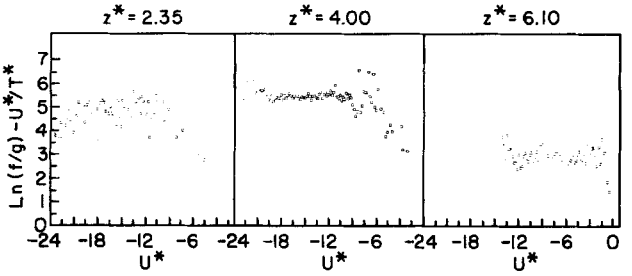


**Figure 8** The ratio algorithm is shown here for the three $z^*$ values of Figures 5 and 7. According to the theory, the values of $\ln(f/g) - u^*/T^*$ should be independent of $u^*$ and equal to $\mu^*/T^*$.

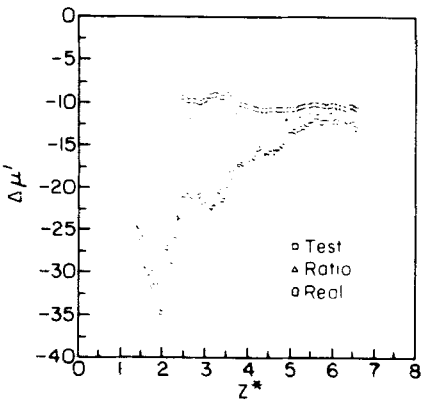


**Figure 9** This plot summarizes the results of the chemical potential calculations using the three algorithms studies here. The dependence of the computed chemical potentials upon $z^*$ are shown for each. These points are based on configurations generated for timesteps 10,000 to 20,000.



layer; 2) the real particle algorithm does not give reliable results; 3) the test particle algorithm is a clear improvement over the real particle but still does not show satisfactory constancy with position; 4) although the ratio method is the most difficult to implement, it appears to produce the best results. In addition, the evaluations of the energy distributions $f(u)$ and $g(u)$ show why there are difficulties in the test and the real particle calculations, since both involve weighted integrals over the distributions that have large contributions from energy regimes where the integrands are quite uncertain. On the other hand, the ratio method requires only that there be a range of energies where accurate values of both $f(u)$ and $g(u)$ can be evaluated. This is the case in our simulated system (with the exception of layer one). When local chemical potentials are calculated from plots such as those shown in Figure 8, the values are independent of $z^*$ except for a small scatter, as shown in Figure 9. We conclude that $\Delta\mu = -12.0 \pm 0.3$ for this model argon multilayer. Although our estimated precision is not high, one must remember that we are studying a system exhibiting very large variations in surface density with $z^*$ -large enough to give rather poor statistics in the low density regions between layers while simultaneously having regions of high density at the "centers" of each layer. Thus, we feel that the calculations presented here provide a stringent test of the abilities of the three algorithms for simulating chemical potential while producing useful new insights concerning the local thermodynamics of an adsorbed multilayer film.

## *Acknowledgments*

This work was supported by a grant from the Division of Materials Research of the National Science Foundation.

## *References*

[1] Patey, G.N., Valleau, J.P., "The Free Energy of Spheres with Dipoles: Monte Carlo with Multistage Sampling," *Chem. Phys. Lett.*, **21**, 297 (1973).

[2] Widom, B., "Potential-Distribution Theory and the Statistical Mechanics of Fluids," *J. Phys. Chem.*, **86**, 869 (1982).
[3] Shing, K.S., Gubbins, K.E., "The Chemical Potential in Dense Fluids and Fluid Mixtures via Computer Simulation," *Mol. Phys.*, **46**, 1109 (1982).
[4] Powles, J.G., Evans, W.A.B., Quirke, N., "Non-destructive Molecular-Dynamics Simulation of the Chemical Potential of a Fluid," *Mol. Phys.*, **46**, 1347 (1982).
[5] Shing, K.S., Gubbins, K.E., "The Chemical Potential from Computer Simulation. Test Particle Method with Umbrella Sampling", *Mol. Phys.*, **43**, 717 (1981).
[6] Knight, J.F., Monson, P.A., "Computer Simulation of Adsorption Equilibria for a Gas on a Solid Surface Using the Potential Distribution Theory," *J. Chem. Phys.*, **84**, 1909 (1986).
[7] Heinbuch, U., Fischer, J. "Model Studies of Adsorption on Plane Interfaces and in Pores", in *Fundamentals of Adsorption*, Ed. A.L. Myers, G. Belfort, (Engineering Foundation, 1987) p. 245.
[8] Bhethanabotla, B., Steele, W.A., "Simulation of the Thermodynamic Properties of Kr Adsorbed on Graphite at 100 K, "*J. Phys. Chem.*, **92**, 3285(1988).
[9] Cheng, A., Steele, W.A., "Computer Simulations of Mono- and Trilayer Films of Argon on Graphite, "*Langmuir*, **5**, 600 (1989).
[10] Hoover, W.G., "Canonical Dynamics: Equilibrium Phase-Space Distributions, "*Phys. Rev. A* **31**, 1695 (1985); Evans, D.J., Morriss, G.P., "Isothermal-Isobaric Molecular Dynamics," *Chem. Phys.*, **77**, 63 (1983).
[11] Rowlinson, J.S., Widom, B., "*The Molecular Theory of Capillarity*", (Oxford University Press, London, 1982).
[12] Allen, M.P., Tildesley, D.J., "*Computer Simulation of Liquids*", (Clarendon Press, Oxford, 1987).
[13] Hansen, J.P., McDonald, I.R., "*Theory of Simple Liquids*", 2nd Ed. (Academic Press, 1987).